Deconvolution of fracture properties of TiN films on steels from nanoindentation load–displacement curves

S. Bhowmick [a], V. Jayaram [a,*], S.K. Biswas [b]

[a] *Department of Metallurgy, Indian Institute of Science, Bangalore 560 012, India*
[b] *Department of Mechanical Engineering, Indian Institute of Science, Bangalore 560 012, India*

Abstract

A columnar TiN film under contact loading fails by shear fracture along inter-columnar boundaries. To deconvolute inter-columnar fracture strength from load–displacement curves, nanoindentation experiments were carried out on columnar ~1.4 μm thick TiN films deposited on steels of various hardness, using a Berkovich indenter. A model, which is developed based on the shear-fracture driven deformation of the coating, is applied to the load–displacement curves to obtain inter-columnar fracture strength. The correlation between the fracture strength, biaxial residual stress and substrate yield stress is outlined. The result suggests that the presence of a high compressive residual stress substantially improves the shear fracture strength of a columnar TiN film.

Keywords: TiN films; Nanoindentation; Shear fracture; Residual stress

1. Introduction

Depth sensing nanoindentation provides fingerprints of a material's properties in terms of load–displacement curves. Over the last two decades, a number of models [1–8] have been developed to analyse load–displacement curves to obtain useful information about the mechanical properties of a bulk material. The ability to deform a material at a small scale makes nanoindentation a useful tool for quantitative characterization of mechanical properties of thin films. Typically for a soft film on a hard substrate, shallow indentations with contact depth < 10% of the film thickness are used to ensure that measurements of the mechanical properties of the film are not affected by the presence of substrate. For a hard film on a soft substrate, such as TiN on steel, the overall response of the system to indentation over a wide range of contact depth is determined by elasto-plastic deformation of the film and the substrate as well as by the fracture of the film. Deconvolution of mechanical properties of the film from such complex deformation mechanisms is indeed a difficult task. This has motivated researchers to undertake extensive experimental [9–20] as well as analytical studies [21–24] of contact mechanisms of hard films on soft substrates.

For indentation loading of a typical elastic and hard thin film on a ductile substrate, the mode of deformation of the film is assumed to be controlled by the plastic deformation of the underlying substrate. Bending and stretching of the film due to yielding of the substrate induce stresses that lead to fracture in the brittle film. Generally the deformation mechanism of TiN film under indentation is strongly influenced by the structural morphology of the coating. The formation of circumferential cracks at the edge of a spherical indentation in columnar TiN films on soft substrates has been reported by Souza et al. [9], while Shiwa et al. [25] and Weppelmann et al.

* Corresponding author. Tel.: +91 802 2933243; fax: +91 802 3600472.
E-mail addresses: qjayaram@met.iisc.ernet.in (V. Jayaram).

Nomenclature

a	radius of contact at the free surface of the film under indentation	t	film thickness
a'	radius of contact at the interface of film/substrate under indentation	P_k	load for elasto-plastic deformation of TiN film
a_o	lattice parameter of the stress-free powder	P_1	load for shear fracture of TiN columns
a_i	lattice parameter of the film	P_2	load for elasto-plastic deformation of substrate
E_f	elastic modulus of TiN film	P_h	$P_1 + P_2$
E_s	elastic modulus of steel	τ^*	critical inter-columnar failure (shear) stress of TiN film
h	indentation depth	θ	semi-apical angle for conical indenter
P	indentation load	ε_z	strain in the thickness direction of the film due to residual stress
σ_s	uniaxial yield stress of steel	υ	Poisson's ratio of the film
σ_f	uniaxial yield stress of TiN film	μ	frictional coefficient between two columns
σ_r	shear yield stress of TiN film		
σ_{res}	residual stress in TiN film		

[26] have shown the appearance of shear faulting cracks along the inter-columnar boundaries under a spherical indenter in a columnar TiN film deposited on brittle substrates. Similar inter-columnar shear fracture in TiN films on ductile substrates have been reported by Ma et al. [27,28] from observations of cross sectional microstructures of an indented zone made by a Vickers indenter. The cross sectional sample of the indented zone prepared by focussed ion beam machining has been used recently to obtain experimental evidence of the deformation mechanism under a spherical indenter of a TiN film on a stainless steel substrate [29]. Microstructural observation of the impression indicated that beyond the elastic deformation of the film, the deformation of the system is dominated by concentric rings of cracks on the coating surface which are formed due to slippage of columns by shear at inter-columnar boundaries.

Unlike in the case of a spherical indenter, a sharp indenter may induce plastic flow in the hard coating itself. This has led to a variety of models to simulate and analyse deformation in the coating and substrate with a view to deconvoluting coating hardness from the composite response of the film and the substrate. One class of models, which uses a rule of mixtures approach assigns a plastically deforming volume to each material and obtains the net hardness by a linear average, was proposed by Buckle [30], Burnett and Page [31], Sargent [32], Jonsson and Hogmark [33] and Burnett and Rickerby [34]. These models also assume tensile cracking of the film at the edge of the impressions during indentation loading of brittle thin films on ductile substrates. However, the applicability of rule of mixture models in analysing deformation of such films may be questioned as it has been shown that the required stress for shear fracture is much lower than the stress for dislocation associated plasticity in columnar TiN films [29]. Thus, when shear fracture dominates deformation, continuum film hardness may not be the most appropriate property to measure even when sharp indenters are used.

The present paper is an extension of our previous study [29] where the nanoindentation loading characteristics of a TiN film on steel were analysed on the basis of experimentally observed morphology of deformation which occurred during Hertzian indentation. Based on these observations, a simple analytical model of the load support mechanism was proposed. It was shown that the predicted loading from the model could be fitted to the experimental load–displacement curve for an adjustable parameter, i.e., an inter columnar shear stress (τ^*) which quantifies the resistance of the film to undergo inter columnar shear fracture in the direction of the column axis [29]. In this analysis the load–displacement response of the system does not reflect plastic flow by dislocation movement in the film. We contend that as long as the hard film remains columnar, the low columnar shear fracture stress dominates the film response for all indenter shapes. The model developed for a spherical indenter is in principle applicable to the analysis of deformation by sharp indenters. We attempt here to validate this belief by indenting columnar TiN films deposited on steel substrates by a sharp tip Berkovich indenter and attempt to predict the load–displacement characteristics using the earlier model corrected for the indenter shape. An important issue addressed here is the role of in-plane residual stress on the fracture property of the film. It has been observed that the presence of biaxial residual stress strongly influences the hardness of the film [35,36]. Here, we demonstrate that the residual stress has an important effect on the fracture behaviour of the film, and that the presence of compressive residual stress is essential to retain the structural integrity of the film.

2. Experimental procedure

TiN films were deposited on three substrates, mild steel (MS), stainless steel (SS) and high speed steel (HSS). The films are strongly textured on {1 1 1} with a columnar structure with columnar diameter of ~0.5 μm. The hardness of MS, SS and HSS were measured by conventional micro-indentation using a Vickers indenter to be 2.5, 5.8 and 9.1 GPa, respectively. TiN films of 1.4 μm were deposited on the substrates using cathodic arc evaporation. The substrates were polished by a succession of polishing papers ending with Buehler micro polishing cloth and a final surface finish of $R_a \sim 0.01$ μm. Prior to deposition, the substrates were cleaned thoroughly with a solvent and dried before being placed on a continuously rotating planetary holder inside the vacuum chamber. The substrates were then heated using radiant heating to the deposition temperature of 350 °C. After the chamber was evacuated to a pressure of 1.3×10^{-3} Pa (10^{-5} Torr), the substrates were sputter cleaned with Ar^+ and coated with a thin layer of Ti (~50 nm) to improve the adhesion of the TiN film. Deposition of TiN was carried out in high purity nitrogen at a pressure of 2.6 Pa (20 mTorr). A negative bias voltage of 150 V was applied to the substrates during deposition. A film thickness of 1.4 μm was achieved after 45 minutes of deposition.

Instrumented nanoindentations were carried out with a displacement-controlled nanoindenter XP (MTS). A Berkovich indenter with a tip radius of 100 nm was used for indentations. A force modulation technique was applied to measure hardness continuously during loading. Cross section sample of the indentation zones were prepared by focused ion beam (FIB) machining. Residual stress measurements of the films were carried out using X-ray diffraction.

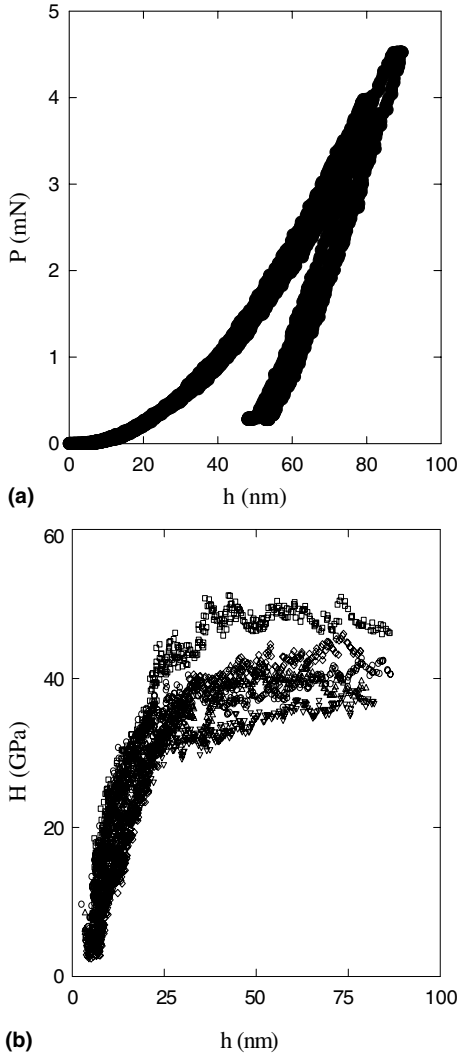

Fig. 1. Nanoindentation (a) load–displacement and (b) hardness–displacement curves of TiN films on SS at low indentation depth.

3. Results

3.1. Nanoindentation curves and images of a contact zone

The results obtained from the depth-sensing force modulation nanoindentation experiments on a TiN thin film (1.4 μm) on SS are shown in Figs. 1 and 2 for two different indentation depths. While Fig. 1(a) shows the typical load–displacement plots at low indentation depth, the corresponding hardness variation, which is measured using the force modulation technique, is displayed in Fig. 1(b). It may be noted that the measured hardness is nearly constant in the 20–80 nm depth range, and the hardness value (35–45 GPa) is similar to the hardness of TiN film reported in the literature [37]. As the depth of indentation is increased, other deformation modes such as elasto-plastic deformation of the film and substrate and fracture damage in the film are expected to influence the load–displacement plots. Fig. 2 shows the load–displacement plots of TiN films on MS, SS and HSS, when the indentation depths are comparable to the film thickness. It may be observed that the experimental curves run together up to a depth of indentation ~200 nm, where the deformation is mainly dominated by the film. As soon as the substrate starts to influence the deformation ($h > 200$ nm), the curves deviate from each other, and at a very high load, they form separate bands of curves for different substrates.

The initial deformation under indentation, which was found to be elastic under a spherical indenter [29], is no longer so under a sharp tip pyramidal indenter. The hardness (Fig. 1(b)) at low indentation depth, which is similar to that of TiN, suggests that the initial deformation is likely to be elasto-plastic deformation of the film due to the high stress developed in a very small region (one or two columns) just under the sharp tip. At higher indentation depths, when the substrate flows plastically,

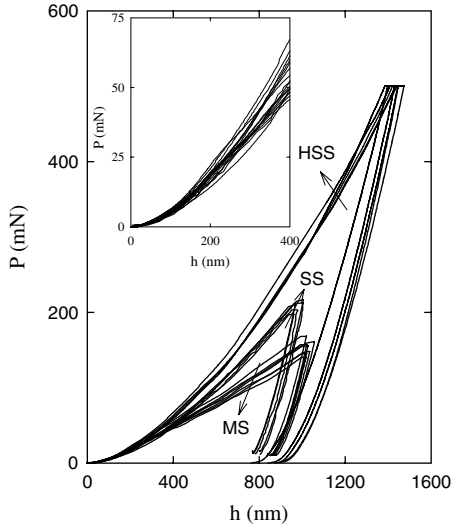

Fig. 2. Nanoindentation load–displacement curves of TiN films on MS, SS and HS; magnified view of load–displacement curves at low indentation depth is shown in inset.

the film is likely to follow the deformed substrate. When there is substantial plastic flow in the substrate, the energy, which is stored in the film because of bending and stretching, is released by breaking the weakest link of the film, i.e., the boundaries between the columns.

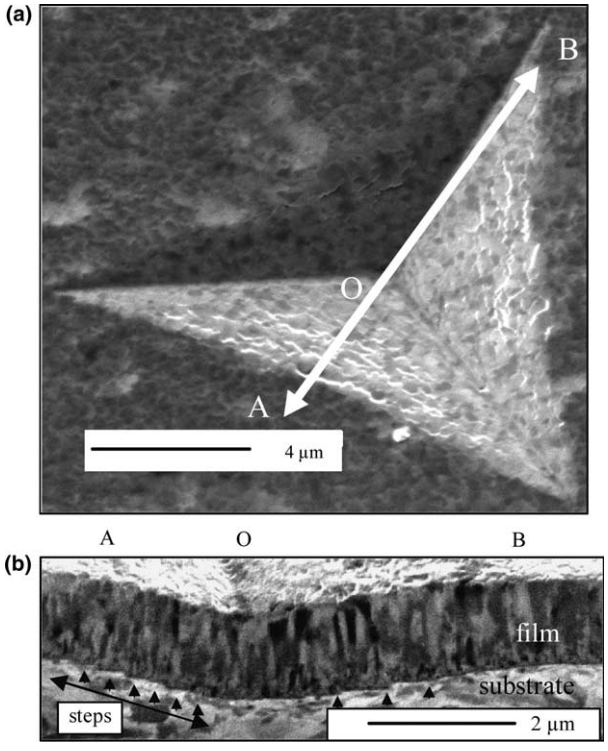

Fig. 3. FIB images of (a) an impression showing the cracks parallel to the edges, and (b) a cross section showing the steps at the film–substrate interface. The cross section sample is prepared by milling the impression perpendicular to 'AB'. Note that the step size in 'AO' in (b) is similar to the column diameter of TiN films because the sectioning is carried out normal to the shear cracks in 'AO'; whereas in 'OB', the step sizes are larger as the section runs almost parallel to the cracks.

Fig. 3 illustrates the FIB images of a typical impression and a cross section at a load of ~500 mN in a TiN film on a HSS substrate. The presence of cracks (spacings ~0.5 μm) parallel to the indentation edge on the coating surface may be observed inside the impression. The appearance of the steps at the film–substrate interface in the cross section micrograph clearly indicates that the cracks on the coating surface are formed due to the slippage of columns by shear at inter-columnar boundaries. We develop below a model for what is essentially the high load response and note the deviation thus introduced in the lower load part of the load–displacement characteristics.

4. Analysis

In this section, a simple analytical model is developed taking the geometry of a sharp tip pyramidal indenter into account. To facilitate modelling using validated contact mechanical formulations, we convert the Berkovich indenter to an equivalent conical indenter by setting up an area equivalence between the spherical and Berkovich indenters using their respective area functions. For a Berkovich indenter with a perfect triangular pyramid geometry, the area function is given by $A(d) = 24.5d^2$ [38] at a distance d from the tip. This area function which is equated to the area (πa^2) of a conical indenter with a semi-apical angle θ, where a is the radius at a distance d, gives a semi-apical angle of ~70° for an equivalent conical indenter [38,39]. It is known that many brittle materials are capable of showing ductile behaviour [40] under sufficiently high pressure such that a plastically deformed zone is formed beneath an indenter. The elasto-plastic deformation, which occurs in a very small region of the film during initial loading, can be modelled by considering the expanding cavity model [41] for elasto-plastic flow of the film. We may write the following equation for initial elasto-plastic deformation of the film under a conical indenter of semi-apical angle θ as [41]

$$P_k = \frac{2\pi(a)^2\sigma_f}{3}\left\{1 + \ln\left(\frac{E_f \cot\theta}{3\sigma_f}\right)\right\}. \quad (1)$$

Substituting $E_f = 400$ GPa [29], and $\theta = 70°$, the estimated loading curve is plotted with the experimental plot. It can be observed in Fig. 4 that the estimated loading curves fit well with the experimental loading curves for a range of $\sigma_f \sim 16$–22.5 GPa (this corresponds to the hardness of 32–45 GPa assuming $H/\sigma_f \sim 2$, as expected for such a hard material [42]), when the displacement remains less than 200 nm.

In the light of our observations of the subsurface zone we assume that at higher indentation depths, the overall deformation is dominated by shear fracture of the film and elasto-plastic deformation of the substrate.

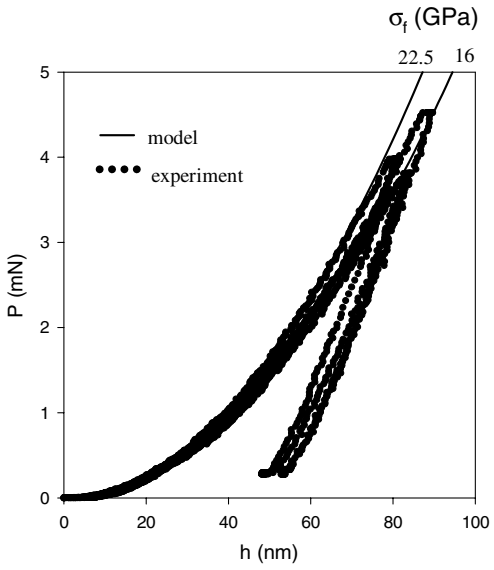

Fig. 4. Estimated loading curves using spherical cavity model with experimental plots at low indentation depth for TiN on SS.

This model has been elaborated before [29] and is briefly reviewed here. When a fixed displacement δ of the indenter is to be implemented in the system, the columns at the edge of the contact displace vertically by δ with respect to the columns outside the contact as shown in Fig. 5. This allows the indenter and the rest of the film which is now attached to the indenter as a cap, to displace vertically by δ and to expand the plastic cavity in the substrate accordingly. Thus for the indenter to displace by δ, it has to overcome (1) the resistance due to inter-columnar shear and (2) the elasto-plastic resistance of the bulk substrate. This mechanism leads us to the model where these two resistances act as two parallel springs undergoing a fixed vertical displacement δ. If they bear loads P_1 and P_2, and total indentation load is P_h, then we can write, $P_h = P_1 + P_2$.

Thus, the load required to fracture the inter-columnar boundary in shear at a distance a from the indentation center is P_1,

$$P_1 = 2\pi a t \tau^*, \tag{2}$$

where t is the film thickness, τ^* is the inter-columnar failure strength in shear. The contact radius, a can be replaced by $h\tan\theta$, where h is the indentation depth. Thus,

$$P_1 = 2\pi\tau^* th\tan\theta. \tag{3}$$

The load required to deform the substrate elasto-plastically under a conical indenter can be defined by the following equation:

$$P_2 = \frac{2\sigma_s\pi(a')^2}{3}\left\{1 + \ln\left(\frac{1}{3}\frac{E_s\cot\theta}{\sigma_s}\right)\right\}. \tag{4}$$

Plastic deformation of the film, which has a strong influence in the loading curve during initial contact, can be argued to have a minimal effect on the overall response once the first shear crack appears in the film at the edge of the contact. Hence, the displacement of the indenter due to plastic flow of the film may be ignored in the model for higher indentation depths. Since the film acts as a cap to the indenter, the new radius of contact at the free surface of substrate under the film can be written as $a' = \sqrt{(h\tan\theta)^2 + 2ht}$. It will also be shown later that the estimated shear fracture strength of the film (τ^*) from the model is much smaller than the shear yield stress for dislocation slip (~11 GPa, since $\sigma_f/\sigma_r = 2$), ruling out the possibility of plastic deformation of the film

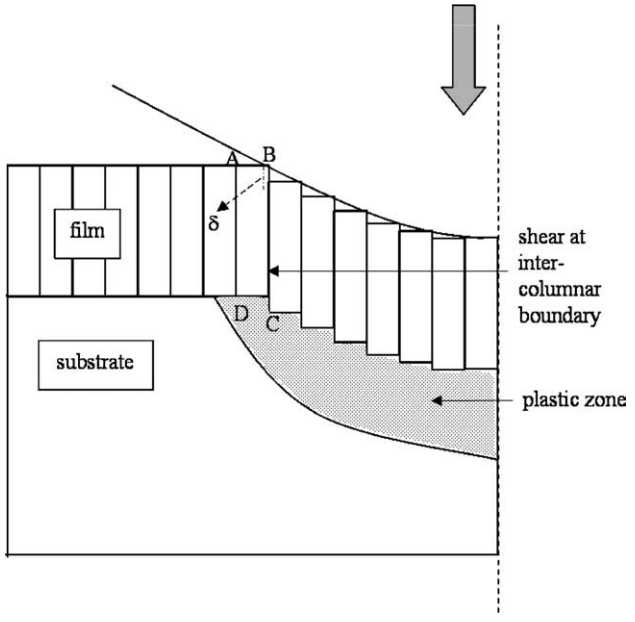

Fig. 5. Schematic of the partitioning of load between the TiN annulus, ABDC, and the expanding cavity in the steel substrate.

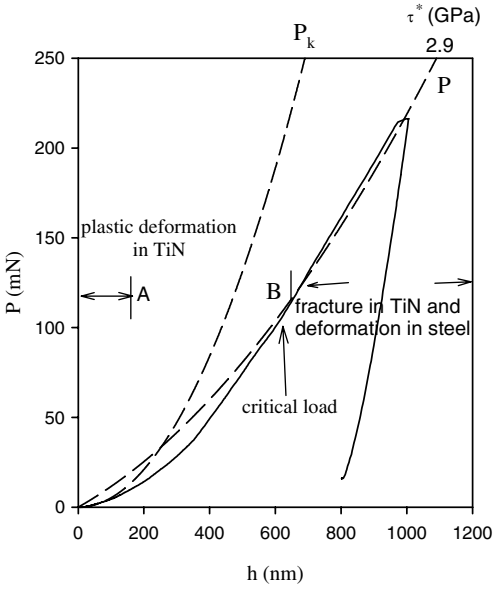

Fig. 6. Experimental curves fitted with estimated load–displacement curves.

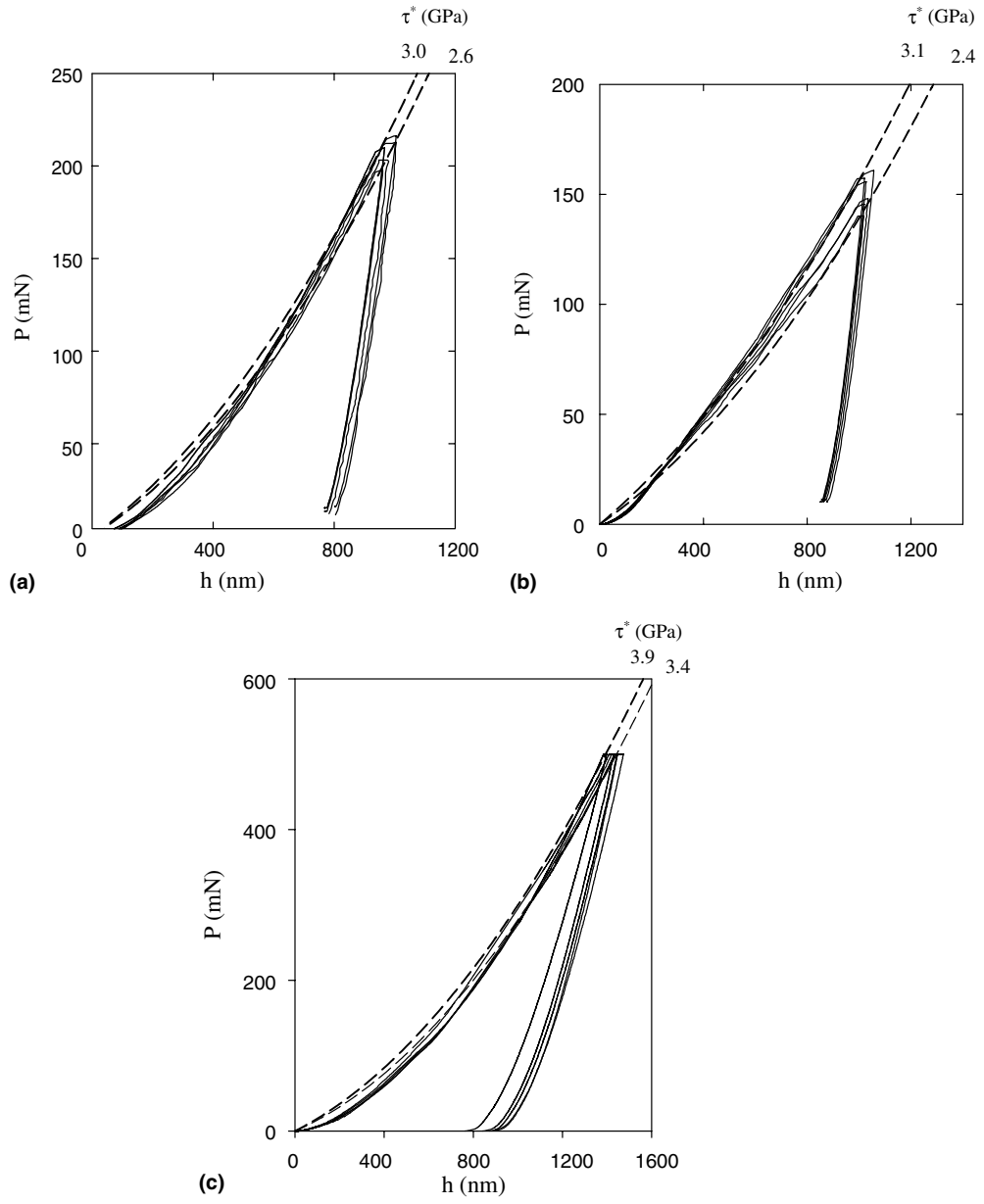

Fig. 7. Experimental curves fitted with estimated load–displacement curves for TiN on (a) SS, (b) MS and (c) HSS.

at higher indentation depths. The deformation modes observed in the present system for the higher load regime can be modelled as follows:

$$P = P_1 + P_2 = [2\pi th\tau^* \tan\theta] + \left[\frac{2\pi\sigma_s((h\tan\theta)^2 + 2ht)}{3}\left\{1 + \ln\left(\frac{1}{3}\frac{E_s\cot\theta}{\sigma_s}\right)\right\}\right]. \quad (5)$$

Using Eq. (5), the estimated loading curve is plotted against the experimental load–displacement curves of TiN films on stainless steel for a $\tau^* = 2.9$ GPa; in Fig. 6. The elastic modulus and yield strength of steel are taken as, $E_s = 210$ GPa and $\sigma_s = 1.9$ GPa. Fig. 7(a) shows that the high displacement part of the experimental P–h curve falls within an envelope of estimated characteristics bounded by $\tau^* = 2.6$ and 3.0 GPa leading to an average τ^* of 2.8 GPa. Since at the initial stage of contact, the mode of deformation is controlled by elasto-plastic deformation of the film, it may be noticed that the model fits the experimental curve only beyond a critical load after which the deformation is mainly dominated by shear fracture of the film and elasto-plastic deformation of the substrate. The critical load, which is indicated by an arrow in the load–displacement plots in Fig. 6, can be considered as a minimum load at which the first fracture in the film is expected to occur. The transition from "low" load behaviour, in which the

expanding cavity model applies to the TiN alone, to the "high" load behaviour that follows the shear fracture model is indicated by the region 'AB' in Fig. 6 in which both types of deformation contribute to a significant degree. The tip shape is a differentiating factor in indentation mechanism only at the early part of the load history; a sharp tip gives rise to plasticity while the response to a blunt tip is generally elastic. In the later part of the load history, this difference becomes minimal where the average strain imposed by a Vickers, spherical and Berkovich indenters are not substantially different. This is reflected in our experimental results where we deconvolute the similar shear fracture strength (τ^*) from the experimental data obtained from indentations by spherical [29] and Berkovich indenters. This similarity not only provides confidence in the data presented in this paper but also establishes that shear fracture is the dominating damage mode in indentation of columnar hard thin films deposited on a soft substrate, irrespective of the tip shape.

In order to explore the influence of substrate yield strength on the fracture strength of the film, the experimental curves are plotted along with the estimated envelopes of load–displacement curves of TiN films on MS and HSS in Figs. 7(b) and (c). The model fits well for ranges of τ^* of 2.4–3.1 GPa for the cases of MS and 3.4–3.9 GPa for HSS. By fitting the individual curves, an average τ^* is found to be 2.6 GPa in the case of MS and 3.7 GPa in the case of HSS. It may be noted that the transition zone described above shifts to higher loads with increasing substrate yield stress. This result is also expected, since shear cracking of the film is driven by substrate plastic deformation and the harder substrate will delay the onset of plastic deformation till higher applied loads. The sequence of deformations under a sharp tip indenter can be considered as plastic deformation of the film at low load, which is followed by plastic deformation in the substrate and fracture in the film. The present results also indicate that the model fits well for a range of τ^* which is unique for each substrate material. We discuss below the possible reason for this variation in the failure stress of the film for different substrates.

5. Discussion

In the case of a bi-layer system, such as TiN film on steel, the mode of deformation changes from a very low load to a high load, and this change in the deformation mode influences the load–displacement curve significantly. The result reported here demonstrates that the low load part of the loading history can be utilised to obtain an estimate of continuum hardness, while structure sensitive information such as inter-columnar shear strength can be obtained by following the high load part of the loading history. As mentioned in the introduction, a number of rule of mixture models have been proposed in the last two decades to characterise the hardness of thin films from the composite hardness. All of the models assume plastic flow of the film under a sharp tip indenter even at higher loads. Detailed experimental evidence of such an assumption beneath the indented surface is however meager. The present study indicates that the deformation of the hard films under contact loading is dominated by through-thickness shear cracks along the inter-columnar boundary, and not by dislocation associated plastic flow of the film. Hence the use of existing rule of mixture models to determine the hardness of a columnar TiN film is physically unsound and may lead to incorrect results.

Turning to the variation of τ^* with change in the underlying substrate material, it may be considered that since the deposition of a film on a substrate always produces some biaxial residual stress in the film which is likely to scale with the yield stress of the substrate, the critical inter-columnar fracture stress is likely to be influenced by the residual stress in the film. Residual stress measurements in the films were carried out using X-ray diffraction. Here, stress-free TiN powder sample was obtained by depositing TiN films on NaCl crystals during the same processing run as the films. Later, the NaCl crystals were dissolved in water and then filtered to obtain TiN powder. X-ray diffraction patterns are shown in Fig. 8 for the powder sample as well as for films deposited on different substrates. {222} planes are chosen to calculate residual stress in the films. Peak shifts can be observed (Fig. 8) in the cases of films compared to that of the powder sample, thereby indicating the presence of residual stress in the film. However, it may be observed that the peak shift in case of HSS is significantly larger than those for MS and SS. The residual stress is calculated from the strain measurement using the following equation. According to Hooke's law, for balanced biaxial stress state (σ_{res}),

$$\varepsilon_z = -\frac{v}{E_f}(2\sigma_{res}). \tag{6}$$

If the lattice parameter of the stress-free powder sample and the film are a_o and a_i, respectively, then the strain in thickness direction (ε_z) can be defined as

$$\varepsilon_z = \frac{a_o - a_i}{a_o}. \tag{7}$$

The biaxial residual stress, σ_{res}, can be calculated from the equation,

$$\sigma_{res} = -\frac{E\varepsilon_z}{2v}. \tag{8}$$

Table 1 shows the lattice parameters of the powder sample and thin films deposited on three different substrates along with the magnitude of the residual stresses and yield stresses of the substrates. It may be inferred

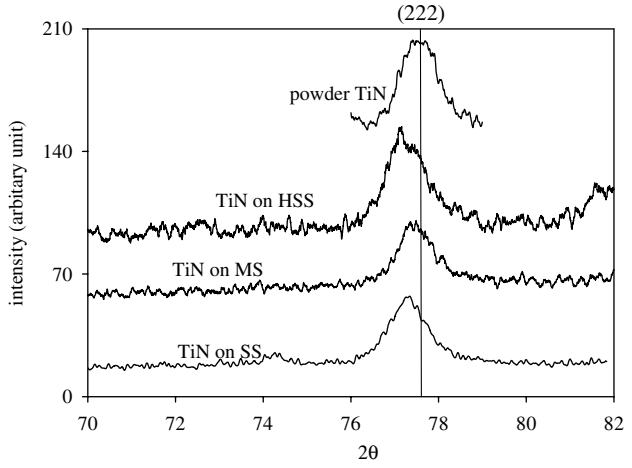

Fig. 8. X-ray diffraction patterns of powder sample and TiN films on MS, SS and HSS.

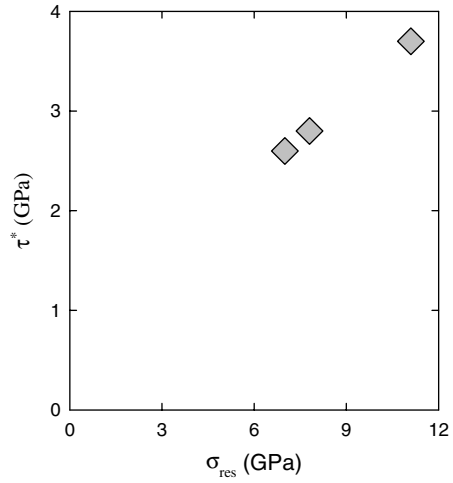

Fig. 10. Plot showing variation of fracture strength with residual stress in the film.

Table 1
List of lattice parameters and residual stresses

Materials	Lattice parameter (Å)	Residual stress (GPa)	Substrate yield stress (GPa)
TiN powder	4.2346		
TiN on MS	4.2643	7	0.8
TiN on SS	4.2677	7.8	1.9
TiN on HSS	4.2816	11.1	3

from the table that the presence of a residual stress increases the estimated τ^*. We therefore conclude that the pre-existing compressive residual stress in the plane of a film increases the resistance to the propagation of shear cracks through the inter-columnar boundaries resulting in an increase in τ^*. The effect of residual stress on τ^* may be illustrated by a simple schematic (Fig. 9). If the friction coefficient between two columns is μ and the residual stress in the film is σ_{res}, then we can write $\tau^*_{res} = \tau^*_0 + \mu\sigma_{res}$, where τ^*_0 is the critical stress for inter-columnar shear fracture when there is no residual stress in the film.

The implication of the influence of residual stress on τ^* presented in this paper is significant in terms of the

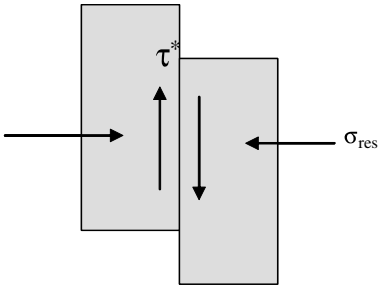

Fig. 9. Schematic showing column sliding under the influence of residual stress.

fracture strength of the films. Since the grain boundaries or columnar boundaries have been identified as the sites of fracture in a columnar thin film, the strength of the grain boundaries can be considered as the strength of the film to fracture. Furthermore, it has been established that the grain boundary strength under contact loading strongly depends on the pre-existing residual stress in the film. Fig. 10, which is drawn on the basis of the present experimental data, implies that a TiN film of zero residual stress may have a very low fracture strength. The data presented here does not have a wide enough range to establish a relationship between residual stress and fracture strength. However, the results clearly indicate that the compressive residual stress induced in these films during deposition is perhaps the single most important factor which provides the high strength to the TiN films to ensure the mechanical integrity of the system.

6. Conclusions

For a film on a substrate system, the deformation mechanism changes gradually from low load to high load and influences the load–displacement curve significantly. The present paper contributes to the analysis of such load–displacement curves on the basis of the deformation mechanism observed in columnar TiN films deposited on steel substrates of various hardness. The following conclusions may be drawn from this study:

1. The initial deformation under a sharp tip indenter is dominated by elasto-plastic deformation of the film and can be simulated using the expanding cavity model for TiN films. The estimated hardness of the film matches well with the hardness obtained from force modulation nanoindentation experiments.

2. Beyond the elasto-plastic deformation of the film, the deformation is dominated by shear fracture of the film along inter-columnar boundaries and plastic flow of the substrates.
3. A simple analytical model is presented for a sharp tip indenter in which the applied load is partitioned between a deforming TiN film and a central expanding cavity in the steel substrate. The model reproduces the experimentally obtained load–displacement curves for an adjustable parameter, namely inter-columnar shear fracture stress (τ^*). An inter-columnar shear fracture strength of 2.8 GPa is obtained for a TiN film deposited on a stainless steel substrate.
4. The shear fracture strength of the film (τ^*) is found to be much smaller than the shear yield stress for dislocation slip, ruling out the possibility of plastic deformation of the film at higher loads where shear fracture dominates the deformation.
5. At higher loads, the loading history is insensitive to tip shape and therefore, similar values of inter-columnar fracture strength are obtained using the models for the indenters of two different geometries, i.e., sharp tip indenter (Berkovich) and spherical indenter.
6. The bi-axial compressive residual stress, which scales with the substrate yield stress, strongly resists the propagation of shear fracture along columnar boundaries. Thus, the presence of a high compressive residual stress provides higher fracture strength of a columnar TiN film.

Acknowledgments

Financial support for this work was made possible by grants from the Defence Research and Development Organisation, Government of India. The samples, which were used in the present study, were prepared at Multi-Arc (India) Ltd. The authors thank Prof. Mark Hoffman (University of New South Wales, Sydney) for providing the FIB facility and Dr. Savio Sebastain (John F. Welch Technology Center, GE, India) for assistance with the nanoindentation experiments.

References

[1] Doerner MF, Nix WD. J Mater Res 1986;1:601.
[2] Oliver OC, Pharr GM. J Mater Res 1992;7:1564.
[3] Field JS, Swain MV. J Mater Res 1993;8:297.
[4] Pharr GM, Oliver WC. MRS Bull 1992(July):28.
[5] Pethica JB, Hutchings R, Oliver WC. Philos Mag A 1983;48:593.
[6] Field JS. Surf Coat Technol 1988;36:817.
[7] Toparli M, Sasaki S. Philos Mag A 2002;82:2191.
[8] Woodcock CJ, Bahr DF, Moody NR. Mater Res Soc Symp Proc 2001;649. Q7.14.1.
[9] Souza RM, Sinatora A, Mustoe GGW, Moore JJ. Wear 2001;251:1337.
[10] Wang JS, Sugimura Y, Evans AG, Tredway WK. Thin Solid Films 1998;325:163.
[11] Li X, Bhusan B. Thin Solid Films 1998;315:214.
[12] Malxbender J, With G, Toonder JMJ. Thin Solid Films 2000;366:139.
[13] Bahr DF, Pang M, Rodriguez-Marek D. Mater Res Soc Symp 2001;649. Q4.2.1.
[14] Cai X, Bangert H. Thin Solid Films 1995;264:59.
[15] Tsui TY, Vlassak J, Nix WD. J Mater Res 1999;14:2204.
[16] Swain MV, Mencik J. Thin Solid Films 1994;253:204.
[17] Weppelmann E, Swain MV. Thin Solid Films 1996;286:111.
[18] Page TF, Hainsworth SV. Surf Coat Technol 1993;61:201.
[19] Lee SL, Wuttiphan S, Hu X, Lee SK, Lawn BR. J Am Ceram Soc 1998;81:571.
[20] Bhowmick S, Kale AN, Jayaram V, Biswas SK. Thin Solid Films 2003;436:250.
[21] Sriram K, Narasimhan R, Biswas SK. Eng Fract Mech 2003;70:1323.
[22] Abdul-Baqi A, Giessen EV. Thin Solid Films 2001;381:143.
[23] Abdul-Baqi A, Giessen EV. J Mater Res 2001;16:1396.
[24] Schwarzer N, Djabella H, Richter F, Arnell RD. Thin Solid Films 1995;270:279.
[25] Shiwa M, Weppelmann ER, Bendeli A, Swain MV, Munz D, Kishi T. Surf Coat Technol 1994;68–69:598.
[26] Weppelmann E, Wittling M, Swain MV, Munz D. Fract Mech Ceram, vol. 12, Bradt RC editor, 1996.
[27] Ma KJ, Bloyce A, Bell T. Surf Coat Technol 1995;76–77:297.
[28] Ma KJ, Bloyce A, Andrievski RA, Kalinnikov GV. Surf Coat Technol 1997;94–95:322.
[29] Bhowmick S, Xie ZH, Hoffman M, Jayaram V, Biswas SK. J Mater Res 2004;19:2616.
[30] Buckle H. In: Westbrook JH, Conrad H, editors. Science of hardness testing and its research applications. Metals Park, OH: ASM; 1973. p. 453.
[31] Burnett PJ, Page TF. J Mater Sci 1984;19:845.
[32] Sargent PM. Microindentation techniques in material science and engineering. In: Blau P, Lawn BR, editors. ASTM Special Technical Publication, 1984, p. 160.
[33] Jonsson B, Hogmark S. Thin Solid Films 1984;114:257.
[34] Burnett PJ, Rickerby S. Thin Solid Films 1987;148:41.
[35] Lee Y, Kwon D. J Mater Res 2002;17:901.
[36] Suresha S, Giannakopoulos AE. Acta Mater 1998;46:5755.
[37] Vaz F, Machado P, Rebouta L, Cerqueira Ph, Goudeau P, Rivière JP, Alves E, Pischow K, de Rijk J. Surf Coat Technol 2003;174–175:375.
[38] Fischer-Cripps AC. Introduction to contact mechanics. Texas: Springer; 2000.
[39] Yoffe EH. Philos Mag A 1982;46:617.
[40] Marshall DB, Lawn BR. In: Blau PJ, Lawn BR, editors. Microindentation techniques in materials science and engineering. Philadelphia: American Ceramics Society for Testing and Materials; 1986. p. 26.
[41] Johnson KL. Contact mechanics. Cambridge: Cambridge University Press; 1985.
[42] Tabor D. In: Blau PJ, Lawn BR, editors. Microindentation technique in materials science and engineering. Philadelphia: American Society for Testing and Materials; 1986. p. 129.